Effect of Composition Profiles on Metallurgy and Corrosion Behavior of Duplex Stainless Steel Weld Metals

Diluting the nitrogen content of the austenite with increased nickel appears to degrade the weld pitting corrosion property

BY T. OGAWA AND T. KOSEKI

ABSTRACT. The weld solidification of duplex stainless steel is entirely ferritic, and the austenite is formed through a solid-state phase transformation during postsolidification cooling. According to the computer-aided microanalysis, the ferritic weld solidification was found to cause the microsegregation of Ni and Mo, that of Ni being more pronounced than that of Mo, although its extent was not so great as compared with the case of austenitic solidification. The partitioning of Cr, Ni and Mo between the ferrite and the austenite was not significant in the welds, while an increase in an austenitizer such as Ni and nitrogen promoted the partitioning by raising the temperature of the transformation to austenite. Nitrogen was found to dominate the formation of the weld austenite by rapid diffusion during post-solidification cooling, being more enriched in the austenite than in that of the base metal.

Preferential occurrence of pitting corrosion within the ferrite in current nitrogen-bearing duplex stainless steel welds is due to the compositionally inferior corrosion resistance of the ferrite and the detrimental effect of precipitates within the ferrite. An increase of nitrogen improves the weld pitting corrosion property by ameliorating the pitting resistance of the austenite of the weld, while an increase of austenite with Ni instead of nitrogen degrades the weld pitting property through the dilution of the nitrogen content in the austenite.

Background and Objectives

Current duplex stainless steels with low carbon and high nitrogen exhibit a good combination of stress corrosion cracking (SCC) resistance, pitting and crevice corrosion resistance, strength, and toughness in comparison with commonly utilized austenitic and ferritic stainless steels (Refs. 1, 2). Therefore, they are being applied increasingly in a variety of fields that contain corrosive, chloride environments, such as oil and gas exploration and gathering systems, pulp and paper plants and chemical processing plants.

The microstructure of wrought duplex stainless steels is established by hot working and subsequent annealing in a two-phase region, and typified by elongated austenite grains in a ferrite matrix. Generally, the proportions of austenite and ferrite are approximately equal in the annealed condition. The above-mentioned property combination of duplex stainless steels mainly results from such a microduplex structure. However, fusion welding processes, which are common methods of fabrication, give rise to quite different microstructures in the fusion and heat-affected zone from that of the base metal, modifying the weld properties adversely (Refs. 3–5).

The solidification of duplex stainless steels is entirely ferritic, with an austenitic phase formed through a solid-state phase transformation during postsolidification cooling (Refs. 3, 6, 7). Thus, the as-solidified microstructure of the fusion zone consists of coarse, epitaxial ferrite grains with inter- and intragranular austenite, though the formation, morphology and resultant content of austenite are justly affected by the weld compositions and welding parameters (Refs. 3, 4, 8, 9). Since the transformation occurs preferentially at prior ferrite grain boundaries, the intergranular austenite generally results in continuous networks and possesses Widmanstatten morphology and/or allotriomorphs, while intragranular austenite, if any, exhibits fine acicular morphology. The adverse effect of such weld microstructures has been particularly pointed out on the localized corrosion resistance in chloride environments (Refs. 4, 5, 9–12). Hence, strong attention has been paid to the localized corrosion behavior of the welds, related to their microstructural characteristics. Pitting corrosion attacks were found predominantly within ferrite in the weld metals, as shown in Fig. 1, which was a striking contrast to the case of base metals where austenite was susceptible to pitting attacks (Refs. 5, 9, 13). The selective pitting corrosion attacks within the weld ferrite were considered to be associated with chromium depletion arising from the precipitation of chromium carbide, carbonitride and nitride within ferrite. The detrimental effect of chromium nitride on pitting corrosion resistance was indicated in weld metals by Sridhar, *et al.* (Ref. 9), in weld heat-affected zones by Ume, *et al.* (Ref. 14), and in cast duplex stainless steels by Poznansky, *et al.* (Ref. 15). However, increased nitrogen certainly exerted a considerable beneficial influence on the weld pitting corrosion resistance (Refs. 4, 11, 16). Furthermore, intergranular austenite was often observed to impede the pit propagation within ferrite in nitrogen-enriched welds, whereas it served as a preferential site of pitting in low-nitrogen welds (Refs. 4, 5, 13). Increased austenite with higher nitrogen improved the weld pitting corrosion resistance, while increased austenite with

KEY WORDS

Duplex Stainless Steel
Composition Profiles
Effect on Metallurgy
Corrosion Behavior
Profile Effects
Weld Microchemistry
Cr/Ni/N_2 Profiles
Weld Transformation
N_2 Transform Control
N_2 Diffusion Effect

T. OGAWA and T. KOSEKI are with the Joining Technology Laboratory, Nippon Steel Corp., Kanagawa, Japan.

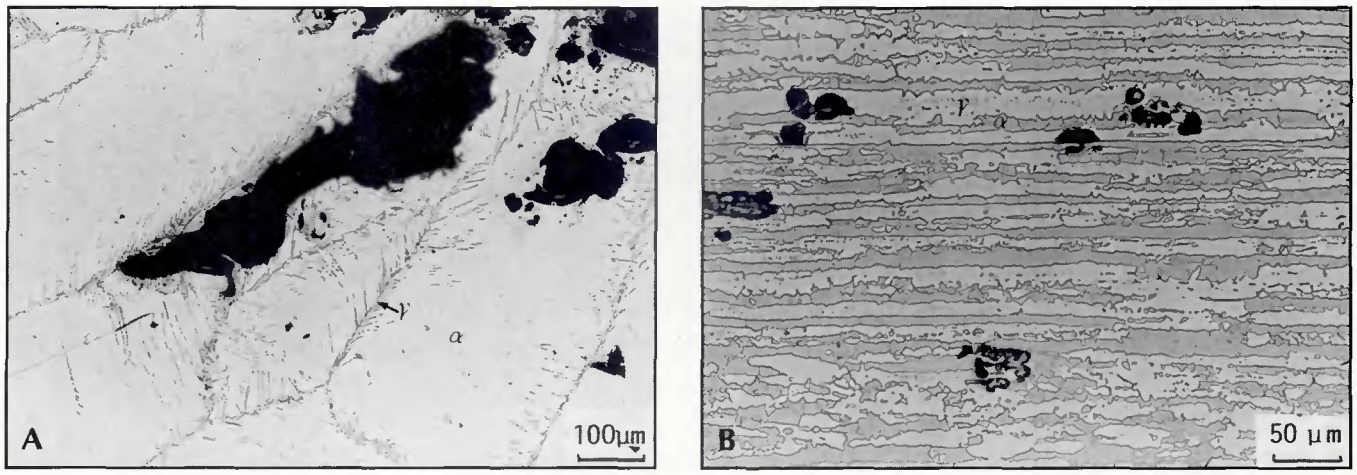

Fig. 1 — Typical pitting corrosion of: A — weld metal and; B — base metal of 22Cr-6Ni-3Mo-0.12N duplex stainless steel. Selective attacks were found in ferrite of the weld metal and in austenite of the base metal

higher Ni content deteriorated when it became too much, though both were effective to diminish the deleterious precipitates within ferrite (Refs. 4, 5, 9). Accordingly, in addition to the detrimental effect of the precipitates, there must be compositional effects on the pitting corrosion behavior in the welds.

As for austenitic stainless steel weld metals, composition profiles in the solidification microstructure have been extensively investigated to understand the solidification sequence (Refs. 17–21), hot cracking (Refs. 22, 23), pitting corrosion (Refs. 24, 25) and fracture (Refs. 26, 27) in the weld fusion zone. On the other hand, only a few studies have been made on the composition profiles in current duplex stainless steel welds, presumably due to their complicated microstructures. Suutala, *et al.* (Ref. 28), indicated that the ferritic solidification was not accompanied by significant segregation, but the solid-state phase transformation to austenite imparted the partitioning of elements between the phases in conventional Cr-Ni-Mo stainless steel welds. Their findings are suggestive, but present no information concerning nitrogen alloying which is essential in currently focused duplex stainless steels. Liljas and Qvarfort (Ref. 16) recently reported the partitioning of major alloying elements, including nitrogen, between the phases in the nitrogen-containing duplex welds by the point-counting technique, using electron probe microanalysis (EPMA). The data showed that the partitioning of Cr, Ni and Mo was, if it occurred, insignificant in the weld metals, while weld nitrogen was partitioned and enriched in austenite to a greater extent than in the case of the base metals. However, since the point-counting measurement gives a limited aspect of composition profiles, full compositional variations relating to weld microstructures remain poorly understood. Nelson, *et al.* (Ref. 29), applied the three-step etching technique to a duplex stainless steel weldment, and successfully obtained the color metallography with regard to the segregation and distribution of Cr throughout the microstructure, but not to those of other elements.

In the present study, the concentration profiles of Cr, Ni, Mo and nitrogen were evaluated in the duplex stainless steel weld metals by using a computer-aided microanalyzer (hereafter referred to as CMA) (Refs. 30, 31). Emphasis was placed on the as-solidified (not heat-affected) fusion zone. The CMA is an EPMA highly computerized in its operation, data acquisition and data analysis. As compared with conventional EPMA, the analytical sensitivity of the CMA is improved by approximately eight times, which facilitated high-speed quantitative analysis of alloying elements in a relatively large area, even as to nitrogen. Moreover, the computerized data acquisition made it possible to analyze and display the data by color graphic images. Based on the composition profiles obtained, the segregation and partitioning behavior of the elements was correlated to the microstructural changes during weld solidification and phase transformation. In addition, the effect of composition profiles on the weld pitting corrosion behavior was discussed.

Table 1—Chemical Compositions of Duplex Stainless Steel Weld Metals Studied

	C	Si	Mn	P	S	Cr	Ni	Mo	N
22Cr-6Ni-3Mo-0.12N	0.013	0.17	1.49	0.013	0.0026	22.52	6.12	3.14	0.127
22Cr-10Ni-3Mo	0.005	0.32	1.49	0.012	0.0063	22.34	9.54	2.98	0.003
22Cr-6Ni-3Mo-0.18N	0.004	0.28	1.50	0.014	0.0065	22.48	6.24	3.01	0.184
22Cr-10Ni-3Mo-0.12N	0.006	0.31	1.46	0.012	0.0064	22.02	9.98	2.91	0.110

Experimental

In order to study the weld microchemistry, four experimental duplex stainless steels containing different amounts of Ni and nitrogen were prepared. The main compositions of the steels were 22Cr-6Ni-3Mo-0.12N, 22Cr-10Ni-3Mo, 22Cr-6Ni-3Mo-0.18N and 22Cr-10Ni-3Mo-0.12N. Those steels were made by vacuum induction melting and hot rolling to 5-mm (0.2-in.) thick plates, and finally annealed at 1050°C (1922°F), followed by water quenching.

Two-pass autogenous (no filler metal added) welding was performed on the plates by the gas tungsten arc welding (GTAW) process. The welding conditions were 200 A and 13 V with a travel speed of 15cm/min (38 ipm). Pure Ar was employed as a shielding gas at a flow rate of 15 L/min (7 cfh). The chemical analyses of the weld metals are given in Table 1. The welded samples were sectioned transverse to the welding direction, and the metallographic examination and microanalysis by CMA were carried out on the surfaces.

The samples were polished and electrolytically etched in a 50% nitric acid aqueous solution for optical microscopy. An area of 200 × 200 μm that exhibited typical microstructure was selected for each sample and marked by microhardness identification. Then the samples were repolished flat prior to microanalysis. The CMA was operated with a beam current of 5 μA at an accelerating voltage of 15 kV. Note that the beam current is markedly increased in CMA as compared with that in conventional EPMA, which is generally in the order of 0.01 to 0.1 μA. The size of an analysis spot was 1 μm, *i.e.*, 200- × 200-μm spots were analyzed step-by-step in each sample. Electron

beam irradiation time for each analysis spot was 200 ms, and during the whole measurement, the variation of beam current was kept within ± 1%.

Ferrite content was measured using a permeability meter (Fischer Feritscope M10).

Results

Composition Profiles of the 22Cr-6Ni-3Mo-0.12N Base and Weld Metal

Figures 2 and 3 show the microstructure and the related CMA images of composition profiles of the 22Cr-6Ni-3Mo-0.12N base metal and its autogenous weld metal, respectively. The microstructure of the base metal consisted of austenite (white) and ferrite (relatively dark), each preferentially elongated to rolling direction, and proportions of the two phases were approximately equal (ferrite: 49%). Ferritizers such as Cr and Mo were significantly enriched in ferrite, while austenitizers such as Ni and nitrogen were enriched in austenite, as generally accepted. The concentration of nitrogen in austenite was approximately 0.2 wt-% on average. On the other hand, the microstructure of the as-solidified fusion zone exhibited coarse ferrite grains with continuous networks of Widmanstatten intergranular austenite. Since the rapid cooling of welding retarded the transformation of ferrite to austenite, the resultant ferrite content was remarkably increased (ferrite: 74%) as compared to that of the base metal. The partitioning of Cr, Ni and Mo was not clear between the two phases, but some locally enriched traces of Ni and Mo were observed in the manner of a periodically arranged network throughout the microstructure of interest. The manner and spacing suggested that such local compositional variation resulted from the segregation of Ni and Mo during cellular/dendritic solidification. Nitrogen was significantly enriched in austenite, more than the case of the base metal, up to 0.3 wt-% on average. Within ferrite, nitrogen was depleted in the vicinity of austenite, while slightly enriched in the region far away from austenite, which was correlated with the nitride precipitation within ferrite, as shown in Fig. 4. It should be noted that the ferrite matrix could contain very low nitrogen content (<0.05 wt-%), as seen in the vicinity of austenite. Figures 5A–D give the distributions of Cr, Ni, Mo and nitrogen within the area examined. The fraction of area, the concentration of which was within a range of interest, was plotted against the mean value of the range, where the increment of the range was selected as 1.0, 0.5, 0.25 and 0.05 wt-% for Cr, Ni, Mo and nitrogen, respectively. As for the base metal, the distribution of all the elements exhibited definitely separated into two maximum peaks due to partitioning between ferrite and austenite, whereas, for the weld metal, the distribution of Cr, Ni and Mo centered on the nominal value with a confined width. Distribution of nitrogen in the weld metal, however, extended to a higher concentration range than that of the base metal.

Composition Profiles of the 22Cr-10Ni-3Mo Weld Metal

Figure 6 shows the microstructure and the composition profiles of the 22Cr-10Ni-3Mo weld metal. Although the calculated nickel equivalent of the weld was almost the same as that of the 22Cr-6Ni-3Mo-0.12N weld, ferrite content was markedly increased to 97% in the as-welded condition. Ferrite/ferrite interfaces without any formation of austenite were observed at some grain boundaries. Composition profiles obviously indicated that partitioning occurred between ferrite and austenite during the austenite formation. Cr and Mo were depleted and Ni was enriched in austenite as is the case of the base metal shown in Fig. 2. Note that the segregation patterns of Ni and Mo were still retained within the ferrite.

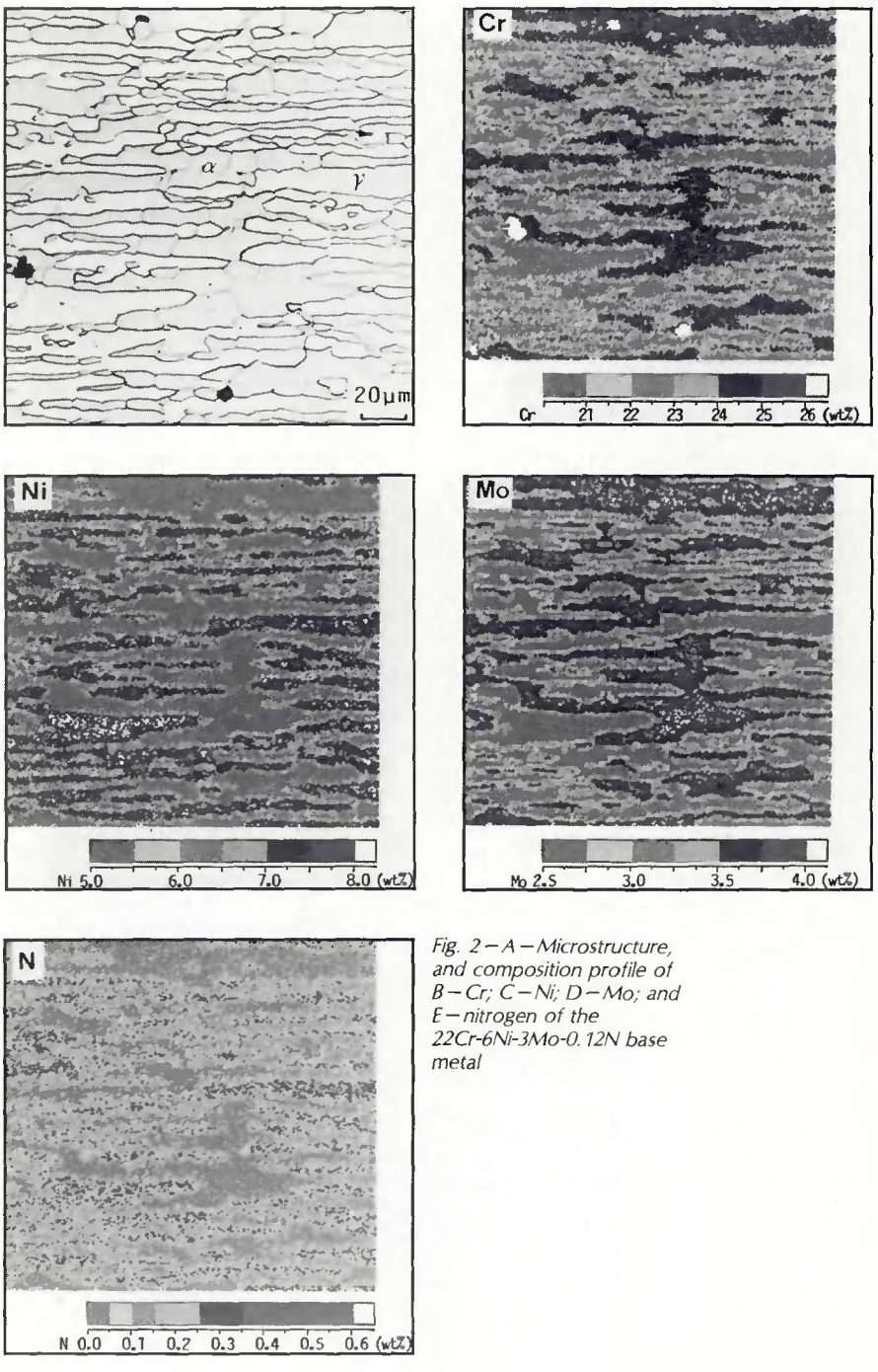

Fig. 2 – A – Microstructure, and composition profile of B – Cr; C – Ni; D – Mo; and E – nitrogen of the 22Cr-6Ni-3Mo-0.12N base metal

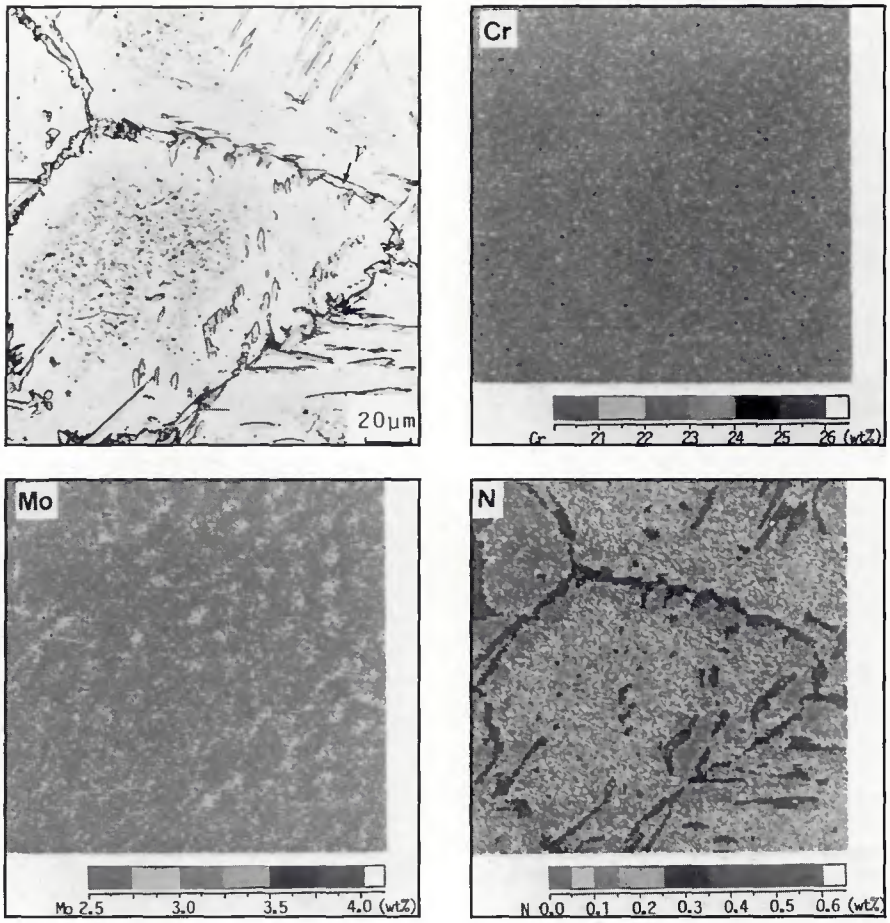

Fig. 3 — A — Microstructure, and composition profile of B — Cr; C — Ni; D — Mo; and E — nitrogen of the 22Cr-6Ni-3Mo-0.12N weld metal

Composition Profiles of the 22Cr-6Ni-3Mo-0.18N Weld Metal

The microstructure and composition profiles of the 22Cr-6Ni-3Mo-0.18N weld metal are given in Fig. 7. Because of increased nitrogen, the ferrite content of the weld was decreased to 49%, and austenite had a well-developed Widmanstatten structure. There was some partitioning of Cr, Ni and Mo, but the concentration difference between the two phases due to partitioning was rather limited as compared with the case of near-equilibrium partitioning found in the base metal. Furthermore, nitrogen was strongly enriched in austenite, up to 0.3 wt-% on average. Also, it should be noted that the nitrogen concentration in austenite of the 22Cr-6Ni-3Mo-0.18N weld was almost the same level as that of the 22Cr-6Ni-3Mo-0.12N weld, though the nominal nitrogen content was increased.

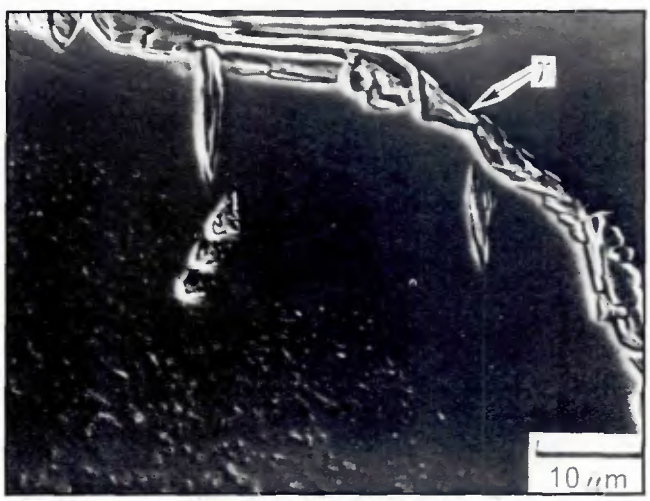

Fig. 4 — SEM micrograph of the 22Cr-6Ni-3Mo-0.12N weld metal, showing austenite at prior ferrite grain boundary and fine, copious precipitates within ferrite. Note the precipitation-free region in the vicinity of austenite

Composition Profiles of the 22Cr-10Ni-3Mo-0.12N Weld Metal

The microstructure and composition profiles of the 22Cr-10Ni-3Mo-0.12N weld metal are displayed in Fig. 8. The weld ferrite content was fairly decreased with Ni content to 25%. The austenite developed with more thickened lath-like morphology rather than the Widmanstatten one into ferrite. Partitioning of Cr and Mo was evident between the two phases, while that of Ni was masked with the segregation pattern, and the correlation of the profile to the microstructure was not well identified. Nitrogen was enriched in austenite, but being diluted with increased austenite; and the concentration (0.2 wt-% on average) was lower than that of the 22Cr-6Ni-3Mo-0.12N weld.

Discussion

Solidification and Transformation of the Weld Metals

The CMA images of composition profiles obtained were quite helpful in understanding the solidification and transformation of the duplex stainless steel weld metals studied.

It is generally accepted that ferritic solidification is not accompanied by

either significant segregation of alloying elements or clearly visible solidification substructures in final weld microstructure due to rapid diffusion and homogenization in ferrite (Ref. 28). However, in the present study, the CMA images showed the evidence of microsegregation of alloying elements resulting from cellular/dendritic solidification. In the 22Cr-6Ni-3Mo-0.12N weld metals, for example, the measured segregation ratios (C_{max}/C_{min}) of Cr, Ni and Mo were 1.05, 1.16 and 1.1 on average, respectively. Although the extent was much lower compared with that in austenitic stainless steel weld metals, it is interesting to note that the segregation certainly remained along the solidification substructures and that of Ni was the most pronounced in the ferritic solidified weld metal. A similar tendency was also ascertained in the 22Cr-10Ni-3Mo and 22Cr-10Ni-3Mo-0.12N weld metals. Fredriksson (Ref. 32) reported the partition coefficient of Ni at the solid/liquid interface during ferritic solidification as 0.84, which is relatively closer to unity than that of Mo (0.80) and thereby indicates less segregation of Ni during solidification (Ref. 33). Thus, the reason for the more pronounced segregation of Ni rather than in Mo should be associated with slower homogenization of Ni during postsolidification cooling. However, because of the great scatters of the reported data on the diffusion of Ni and Mo and the lack of data on the interaction between elements during homogenization in ferrite, the reason still remains uncertain. Nitrogen may be completely homogenized in ferrite just after solidification due to the very rapid diffusion rate.

Just after the solidification, duplex stainless steel attains a ferritic single phase which then undergoes a solid-state transformation to austenite (Refs. 3, 6, 7). According to the delato metric measurement, the transformation of the 22Cr-6Ni-3Mo-0.12N weld occurred approximately at the temperature range of 1250° to 1150°C (2282° to 2102°F) on weld cooling. The diffusion rate of Cr, Ni and Mo would be fairly decreased at that stage, resulting in insignificant partitioning of those elements between the phases. Note that the retained segregation patterns did not affect the austenite formation. Nitrogen, on the contrary, possesses a diffusion rate rapid enough to accelerate the transformation still at the temperature range, resulting in a remarkable increase of nitrogen in the austenite, as shown in Fig. 3E. Therefore, it should be concluded that nitrogen plays the most important role for the austenite formation in nitrogen-containing duplex stainless steel weld metals. This was supported by the fact that the nitrogen-containing weld metal (22Cr-6Ni-3Mo-0.12N) exhibited more increased austenite con-

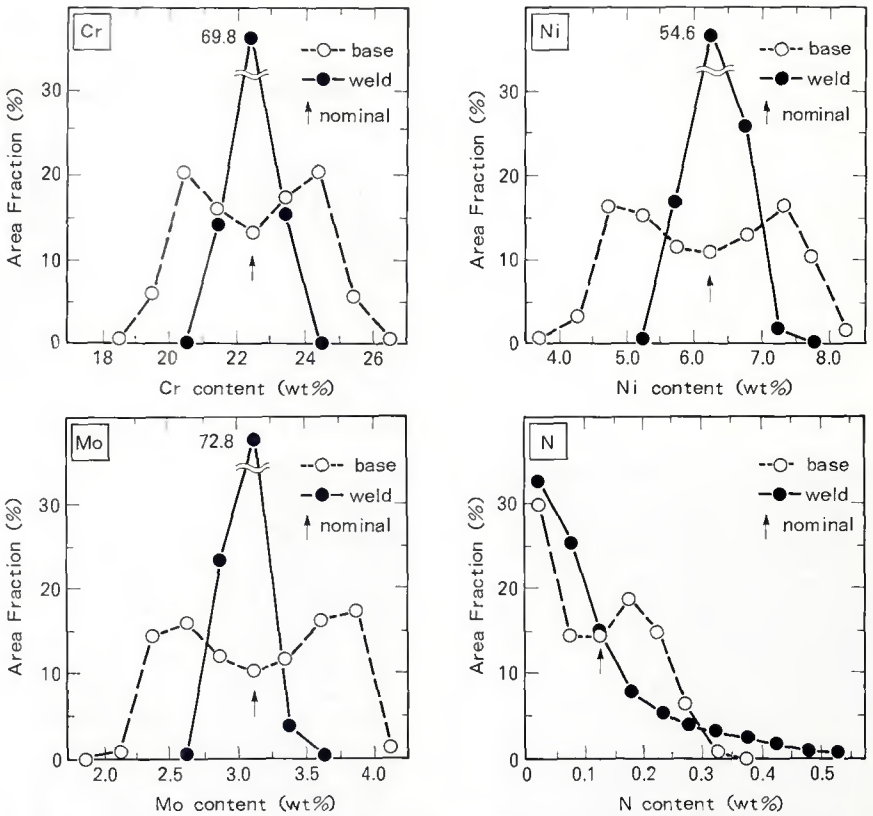

Fig. 5—Distribution of alloy content of: A—Cr; B—Ni; C—Mo; and D—nitrogen within the examined area of the 22Cr-6Ni-3Mo-0.12N base and weld metal

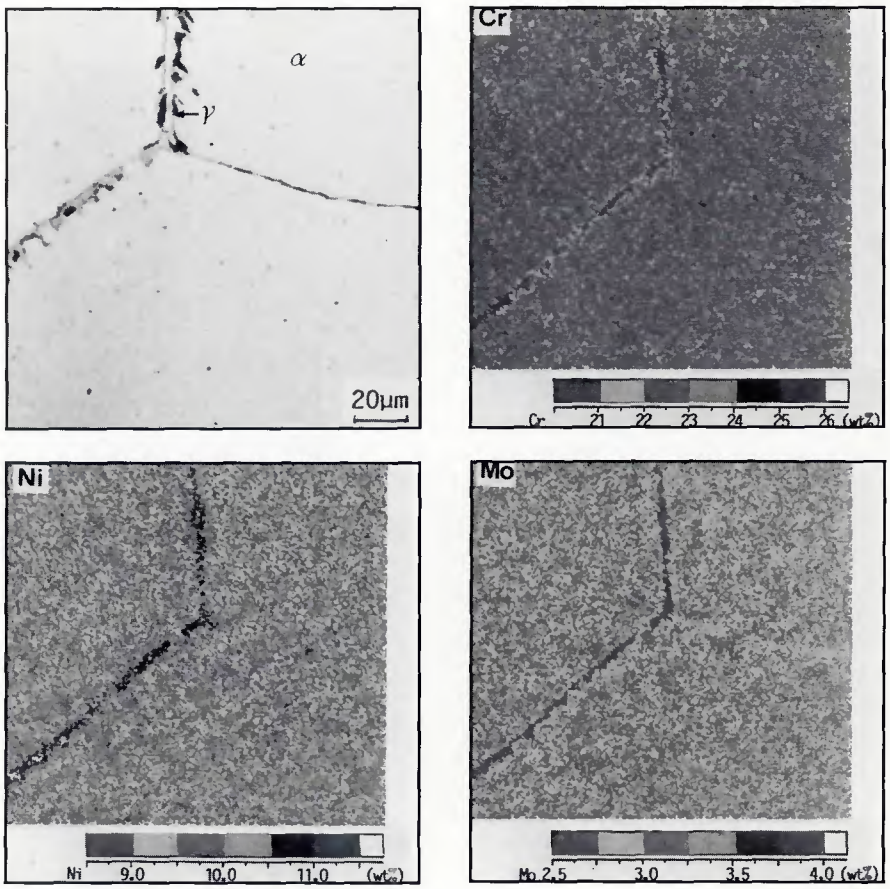

Fig. 6—A—Microstructure, and composition profile of B—Cr; C—Ni; and D—Mo of the 22Cr-10Ni-3Mo weld metal

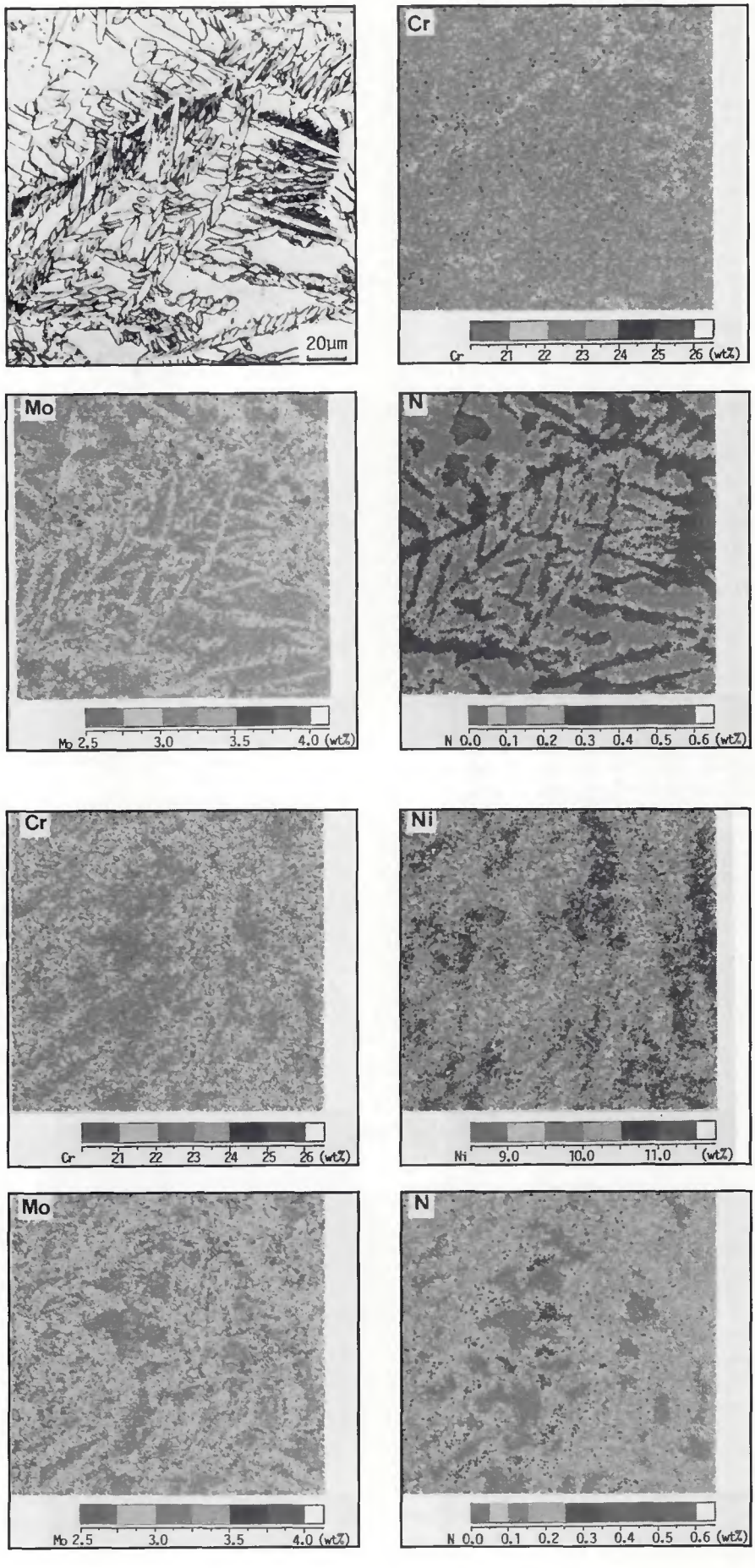

Fig. 7—A—Microstructure, and composition profile of B—Cr; C—Ni; D—Mo; and E—nitrogen of the 22Cr-6Ni-3Mo-0.18N weld metal

Fig. 8—A—Microstructure, and composition profile of B—Cr; C—Ni; D—Mo and E—nitrogen of the 22Cr-10Ni-3Mo-0.12N weld metal

tent as compared to the weld metal of the same Ni equivalent without nitrogen addition (22Cr-10Ni-3Mo). Because of less contribution of Ni to austenite formation, nitrogen is required to be more enriched in austenite for the phase stability in the nitrogen-containing weld as compared with the case of the base metal, and this was certainly attained due to the rapid diffusion of nitrogen. On the other hand, in the case of the no-nitrogen-added weld, the partitioning of Cr, Ni and Mo is indispensable to form and stabilize austenite. Thus, if it occurs, the transformation to austenite is suppressed, as shown in Fig. 6A, due to the slower diffusion rates of those substitutional elements.

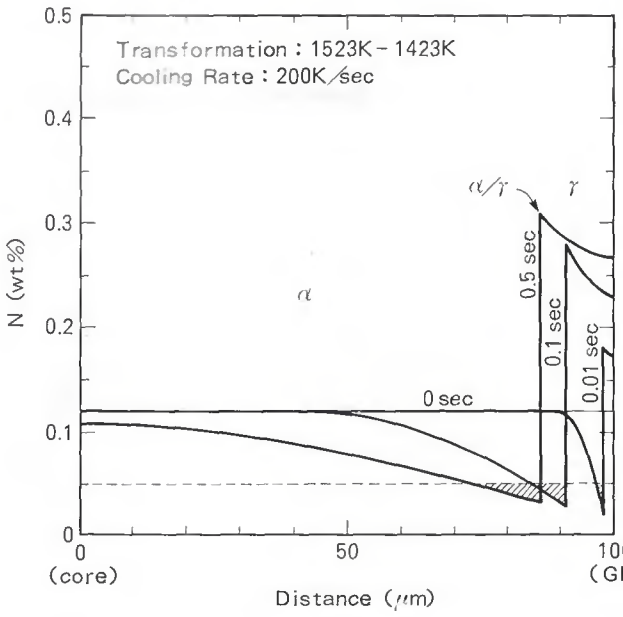

Fig. 9 — Redistribution of nitrogen during ferrite to austenite transformation in the high-N duplex stainless steel weld metal, obtained by numerical calculation

Calculated Distribution of Nitrogen in the 22Cr-6Ni-3Mo-0.12N Weld

It is quite important to note that the transformation process of the weld was predominantly controlled by the diffusion of nitrogen. When the transformation occurs preferentially at prior ferrite grain boundaries, nitrogen diffuses into and stabilizes the intergranular austenite with a rapid diffusion rate, which will lead to the depletion of nitrogen in a ferrite matrix. But, according to the nitrogen profile of the 22Cr-6Ni-3Mo-0.12N weld, the depleted regions existed only in the vicinity of austenite. Limited nitrogen-depleted regions were presumably due to a higher weld cooling rate and larger prior ferrite grain size, which was suggested by the simple calculation model on the nitrogen distribution, taking into account the movement of α/γ interface during transformation. The calculation assumed 1) cylindrical prior ferrite grain, 2) transformation from the grain boundary toward the center with a concentric, planar interface, and 3) the completely diffusion-controlled process of nitrogen. The third assumption means that the system considered was sufficiently undercooled to make the ferrite thermodynamically unstable, and that the diffusion of nitrogen into austenite was the only, and sufficient, requirement for the austenite growth. The governing equations and the initial and boundary conditions are given in the appendix. The moving-grid method of Murray and Landis (Ref. 34) was applied for the numerical solution by the finite difference method (FDM). Regarding the temperature-dependent diffusion coefficient of nitrogen, data in pure α and γ iron (Ref. 35) were used for simplicity. A transformation temperature range of 1250° to 1150°C, a grain size (diameter of cylinder) of 200 μm, and a weld cooling rate of 200°C/s (360°F/s) were employed to fit the conditions to actual ones. The result obtained is depicted in Fig. 9. As the interface moved to the inside of the ferrite grain, the nitrogen-depleted region was found to expand in front of the interface into the ferrite. However, due to the large grain size, the very short time for the transformation, and the decreased diffusion rate with lowered temperature, the central region of the grain was still enriched in nitrogen. Although the model contained some assumptions, the result was consistent with the actual profile of nitrogen. The nitrogen-depleted region seen in Fig. 3E was the result of the migration of nitrogen during the transformation into the adjacent austenite, which behaved as a sink for nitrogen. Enriched nitrogen at the central region of the ferrite grain would result in nitride precipitation below the transformation temperature range. From the calculations with different conditions of grain size and cooling rate, it was indicated that a decrease in grain size and/or cooling rate was effective to decrease the nitrogen content at the central region of the ferrite grain, *i.e.*, to reduce the nitride precipitation within ferrite.

Effect of Increased Ni and Nitrogen on Composition Profiles

In the 22Cr-6Ni-3Mo-0.18N weld metal, nitrogen was highly enriched in austenite, and thus, the postsolidification transformation of ferrite to austenite was supposed to be strongly affected by the diffusion of nitrogen, as in the case of the 22Cr-6Ni-3Mo-0.12N weld metal. But the composition profiles revealed the partitioning of Cr, Ni and Mo between ferrite and austenite in this weld. Owing to increased nitrogen, intergranular austenite nucleated and developed with smaller spacings by the Widmanstatten mechanism, which facilitated the partitioning of the substitutional elements, despite the slower diffusion rate. Moreover, based on the delato metric measurement, increased nitrogen to 0.18 wt-% led to raising the transformation temperature range by approximately 80°C (144°F). A higher transformation temperature also gave rise to the partitioning of substitutional elements by increasing the diffusion rate, though the extent was not so large due to the rapid weld cooling.Thermodynamically, increased nitrogen was stated to suppress the partitioning of Cr, Ni and Mo between the phases in duplex stainless steels (Ref. 36). It is interesting to note that the result obtained in the weld metals was in contrast with the thermodynamical prediction. Kinetic factors such as diffusion and austenite growth are more influential to the partitioning of the elements in the as-solidified weld metals.

On the other hand, in the 22Cr-10Ni-3Mo-0.12N weld metal, the enriched level of nitrogen in the austenite was found to be relatively reduced. The average nitrogen concentration of 0.18 wt-% in the austenite was certainly higher than the nominal concentration of 0.12 wt-%, but not so significant as compared with that of 0.3 wt-% measured in the austenite of other nitrogen-containing weld metals. Because of increased Ni to 10 wt-% in the matrix, the formation and the stability of the austenite on weld cooling should be affected not only by nitrogen, but by Ni. Therefore, with the aid of Ni, nitrogen was not required to be enriched up to a level of 0.3 wt-% for the austenite stability, and was consequently diluted down to 0.18 wt-%. Since an increase in Ni content raised the transformation temperature in the same manner as nitrogen, the partitioning of Cr and Mo could readily occur. However, the partitioning of Ni was indefinitely masked with the segregation pattern, because an increase

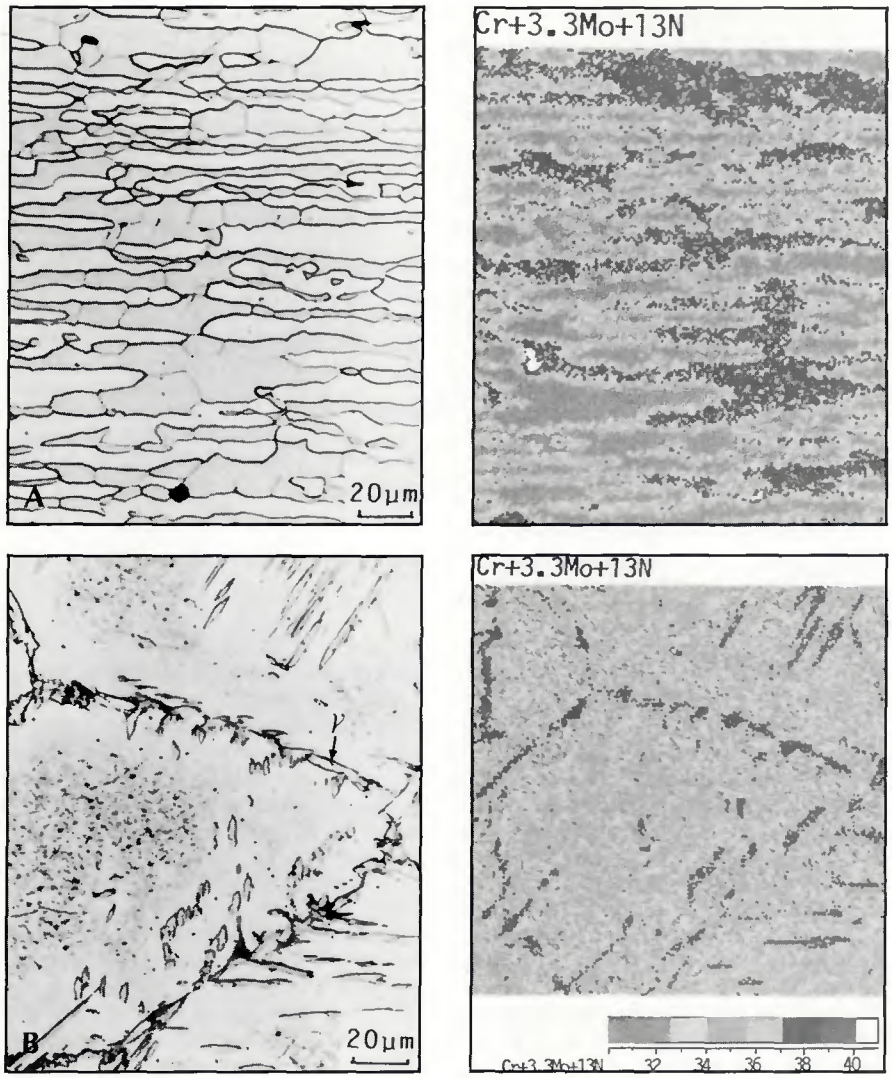

Fig. 10—Profile of the pitting index value (Cr+3.3Mo+13N) in A—base metal and B—weld metal of the 22Cr-6Ni-3Mo-0.12N duplex stainless steel

in the content accompanied more pronounced segregation. Note that the austenite formation and growth was not justly associated with the segregation of Ni.

Effect of Composition Profiles on Weld Pitting Corrosion Behavior in Chloride Solution

It is generally accepted that Cr and Mo are the major elements that improve the pitting corrosion resistance of stainless steels in a chloride environment. As for austenitic stainless steel, the beneficial effect of nitrogen is also documented (Refs. 37, 38). The pitting corrosion resistance of solution-annealed stainless steels has been well-correlated with the nominal content of those elements by using an equivalent, *i.e.*, so-called pitting index, such as Cr+3.3Mo+13N (Ref. 39). In austenitic stainless steel weld metals, the occurrence of pitting corrosion is associated with the minimum levels of those elements at the dendrite cores, which result from the microsegregation during solidification (Refs. 24, 25). Therefore, the compositional effect on the pitting corrosion in duplex stainless steels and their weld metals, which possess composition variation due to segregation and partition, could be understood by considering the microdistribution of the pitting index value (Cr+3.3Mo+13N) throughout the microstructure of interest.

Figures 10A and B give the profile of the pitting index value in the microstructure of the 22Cr-6Ni-3Mo-0.12N base and weld metal, respectively. These images were graphically synthesized on the basis of the composition profiles of Cr, Mo and nitrogen. In the base metal, the ferrite exhibits a higher index value than the austenite because of enriched Cr and Mo by partitioning. Although the austenite is substantially enriched in nitrogen, the depletion of Cr and Mo leads to

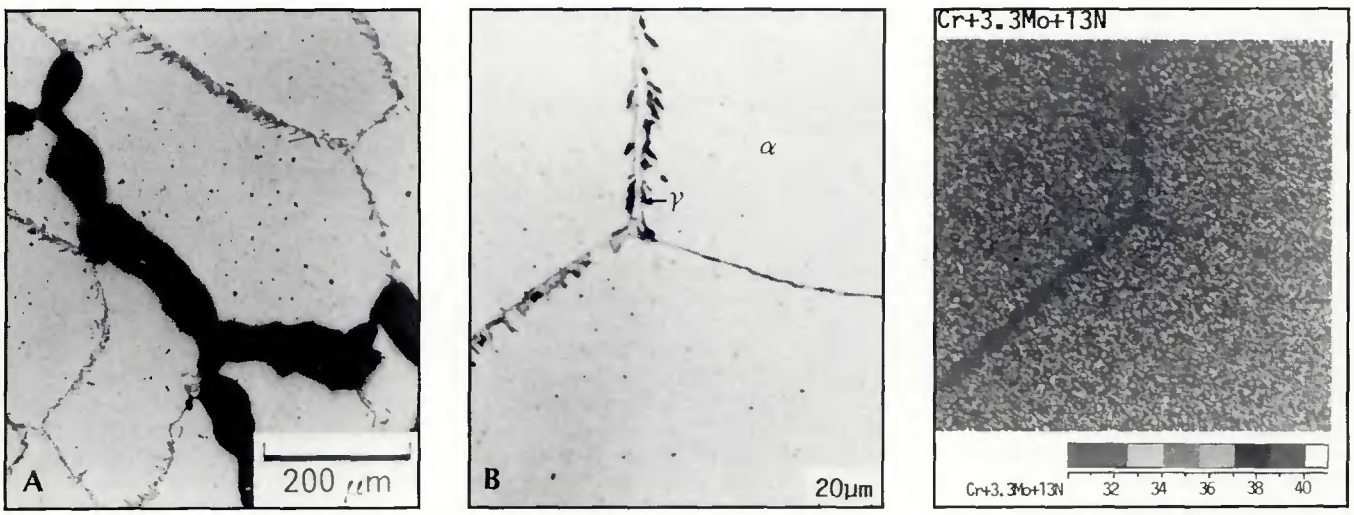

Fig. 11—A—Pitting corrosion and B—profile of the pitting index value (Cr+3.3Mo+13N) in the 22Cr-10Ni-3Mo weld metal

a lower index value, which indicates that the austenite is more susceptible to pitting corrosion. Actually, the austenite was selectively attacked in a chloride solution, as shown in Fig. 1B. On the contrary, the austenite exhibited a higher pitting index value than the ferrite in the weld metal, owing to less partitioned Cr and Mo between the phases and to significantly enriched nitrogen in the austenite. Resulting from Cr nitride precipitation, the central regions of the ferrite exhibit a little higher pitting index value compared with the other ferrite regions, but strictly speaking, those regions would be more susceptible to pitting corrosion than the other ferrite regions because of the precipitates. Thus, in the weld metal, pitting corrosion would occur preferentially in the ferrite associated with either the precipitation or low pitting index value, as shown in Fig. 1A, while, being compositionally noble, the austenite is more resistant to pitting and behaves as an impedient for the pit propagation. The change of corrosion mode between the base and weld metal can be explained compositionally by the change of the profile of the pitting index value arising from different partitioning behaviors of Cr, Mo and nitrogen between the base and weld metal. Note that such change of corrosion mode is characteristic of nitrogen-bearing duplex stainless steels, and this is ascertained by the pitting corrosion behavior of the 22Cr-10Ni-3Mo weld. As shown in Fig. 11, pitting corrosion occurred preferentially in the austenite, even in the weld, when the weld does not contain a substantial amount of nitrogen. The preferable effect of nitrogen on the pitting corrosion resistance of austenite should be noted again.

Figure 12 shows the effect of ferrite content on the chloride pitting corrosion resistance of duplex stainless steel weld metals having the composition of 22 wt-% Cr, 3 wt-% Mo and various amounts of Ni and nitrogen, which was previously reported by the authors (Ref. 5). Different weld ferrite contents were attained by varying the weld Ni content for each nitrogen level. As for the weld metals with 0.12 wt-% nitrogen, the resistance was the most improved around a ferrite content of 50%, and deteriorated in both, more to the ferritic side with lower Ni, and more to the austenitic side with higher Ni. Increased nitrogen, however, improved the resistance of more austenitic weld metals. The decrease in pitting corrosion resistance on the ferrite-rich side is due to the enlarged precipitation area with increased ferrite. In this case, the beneficial effect of an increase in the austenite content on the weld pitting corrosion resistance is attributed to reducing the detrimental precipitation and increasing the corrosion-resistant area with highly soluble nitrogen. How-

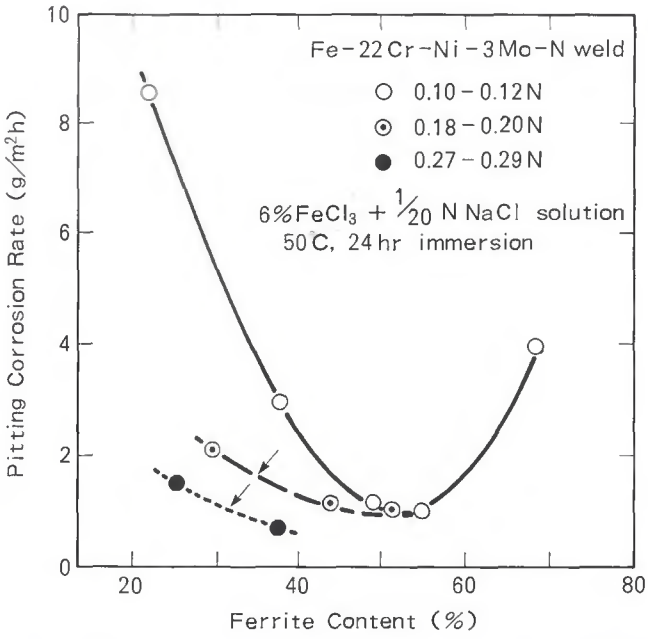

Fig. 12—Effect of ferrite and nitrogen content on pitting corrosion resistance of duplex stainless steel weld metals

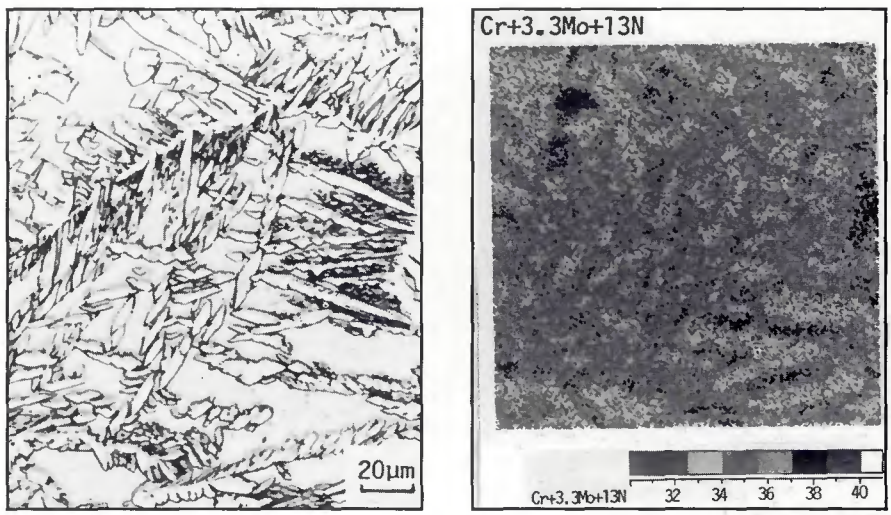

Fig. 13—Profile of the pitting index value (Cr+3.3Mo+13N) in the 22Cr-6Ni-3Mo-0.18N weld metal

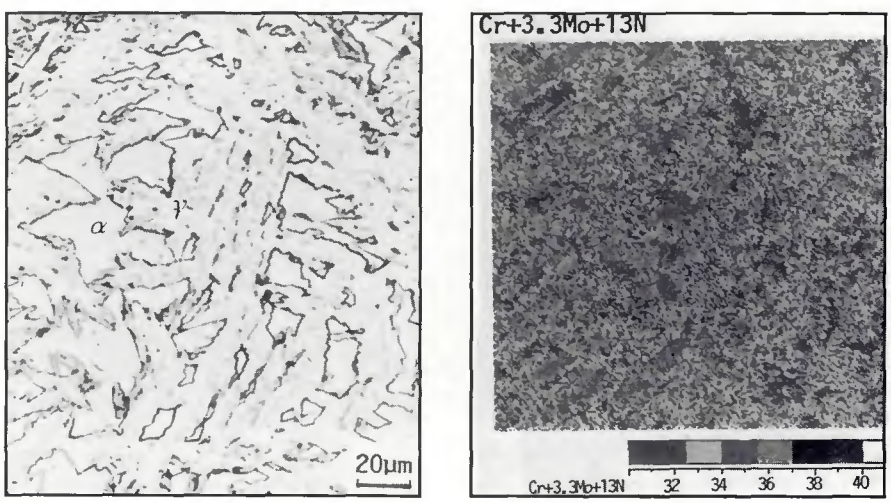

Fig. 14—Profile of the pitting index value (Cr+3.3Mo+13N) in the 22Cr-10Ni-3Mo-0.12N weld metal

ever, the degradation of the pitting corrosion resistance of austenite-enriched weld metal and the preferable effect of increased nitrogen in that case cannot be explained in terms of the precipitation, because increased austenite significantly suppresses the precipitation of carbide and nitride.

Figures 13 and 14 give the profile of the pitting index value within the 22Cr-6Ni-3Mo-0.18N and 22Cr-10Ni-3Mo-0.12N weld microstructures, respectively. The austenite of both welds exhibits a higher pitting index value than the ferrite, but the austenite of the 22Cr-6Ni-3Mo-0.18N weld shows more increased value compared with that of the 22Cr-10Ni-3Mo-0.12N weld due to a more enriched nitrogen content. In other words, increased austenite with higher Ni content results in a lower pitting index value with diluted nitrogen in the 22Cr-10Ni-3Mo-0.12N weld. Since the nitrogen-enriched austenite with a higher pitting index value can offer improved resistance and behave as an impediment to pitting corrosion, the austenite of the 22Cr-10Ni-3Mo-0.12N weld offers a degraded resistance to pit propagation once pitting occurs. Pitting corrosion resistance, shown in Fig. 12, substantially includes the effect of pit propagation, and thus, the degradation of pitting corrosion resistance in welds with higher Ni can be compositionally explained by the dilution of nitrogen in increased austenite. It should be concluded that the pitting corrosion resistance of austenite-enriched duplex weld metals is mainly dominated by the nitrogen content in austenite.

Conclusions

Composition profiles of Cr, Ni, Mo and nitrogen were investigated in duplex stainless steel weld metals having the composition of 22 wt-% Cr, 3 wt-% Mo and different amounts of Ni and nitrogen. Based on the results, the solidification and the phase transformation on welding and the correlation with the pitting corrosion behavior of the welds were clarified. The conclusions obtained are as follows:

1) The ferritic weld solidification was found to cause the microsegregation of Ni and Mo, with that of Ni being more pronounced than that of Mo, although the extent was not so great as compared with the case of austenitic solidification.

2) Partitioning of Cr, Ni and Mo between the ferrite and the austenite is not significant in the nitrogen-bearing welds, but an increase in an austenitizer such as Ni and nitrogen prompts it by raising the temperature of the transformation to austenite.

3) Nitrogen is found to dominate the formation of weld austenite by the rapid diffusion during postsolidification cooling, being more enriched in the austenite than that of base metals.

4) Preferential occurrence of pitting within the ferrite in the nitrogen-bearing welds is due to the compositionally inferior corrosion resistance of the ferrite and the detrimental effect of precipitates within the ferrite.

5) An increase of nitrogen improves the weld pitting corrosion property by ameliorating the pitting resistance of the austenite of the weld, while an increase of austenite with Ni instead of nitrogen degrades the weld pitting corrosion property by diluting nitrogen content in the austenite.

Acknowledgments

The authors wish to thank Mr. Yamanishi for his skillful operation of the CMA, and Mr. Hamada for technical discussions on the CMA data analysis.

References

1. DeBold, T. A., Martin, J. W., and Tverberg, J. C. 1983. Duplex stainless offers strength and corrosion resistance. *Duplex Stainless Steels,* ASM, pp. 169–189.

2. Clark, C. A., and Guha, P. 1983. Improvement in corrosion resistance mechanical properties and weldability of duplex austenitic/ferritic steels. *Werkstoffe und Korrosion* 34:27–34.

3. Gooch, T. G. 1983. Weldability of duplex ferritic-austenitic stainless steels. *Duplex Stainless Steels,* ASM, pp, 573–602.

4. Ogawa, T., Koseki, T., Nagatani, T., and Sakurai, H. 1986. Corrosion resistance and mechanical properties of duplex stainless steel weldments. *Pulp and Paper Industry Problems* 5: 133–137.

5. Ogawa, T., and Koseki, T. 1986. Metallurgical investigation of weldments in nitrogen-enriched duplex stainless steels. *3rd Int. Conf. Welding and Performance of Pipelines.* The Welding Institute, Abington, England, Paper-10.

6. Solomon, H. D. and Devine, Jr. T. M. Duplex stainless steels—a tale of two phases. *Duplex Stainless Steels* ASM, pp. 693–756.

7. Nelson, D. E., Baeslack III, W. A., and Lippold, J. C. 1986. An investigation of weld hot cracking in duplex stainless steels. *Welding Journal* 66(8):241-s to 250-s.

8. Mundt, R., and Hoffmeister, H. 1985. Effect of chemical composition and weld thermal cycles on phase transformation and microstructures of ferritic-austenitic steels. *Proc. Conf. Stainless Steels '84.* The Institute of Metals, pp. 315–321.

9. Sridhar, N., Flasche, L. H., and Kolts, J. 1984. Effect of welding parameters on localized corrosion of a duplex stainless steel. *Mater. Perform.* 23(12):52–55.

10. Kolts, J., Flasche, L. H., Agarwal, D. C., and Tawancy, H. M. 1982. Microstructural effects on the corrosion resistance in a duplex stainless steel in the wrought and welded conditions. *Corrosion Forum '82.* Houston, Tex. NACE Paper No. 190.

11. Pleva, J., and Nordin, S. 1983. Properties of different MMA-welds on modified 329 ferritic-austenitic stainless steel. *Duplex Stainless Steels,* ASM, pp. 603–629.

12. Redmerski, L. S., Eckenrod, J. J. and Kovach, C. W. 1983. Crevice corrosion of stainless steel welds in chloride environments. *Mater. Perform.* 22(6):31–39.

13. Sridahar, N., and Kolts, J. 1987. Effects of nitrogen on the selective dissolution of a duplex stainless steel. *Corrosion.* 43(11):646–651.

14. Ume, N. Seki, N. Naganawa, Y. Hyodo, T. Satoh, K., and Kuriki, Y. 1987. Influence of thermal history on the corrosion resistance of duplex stainless steel linepipe. *Mater. Perform.* 26(8):25–31.

15. Poznansky, A. Nalbone, C. S., and Crawford, J. D. 1983. The corrosion resistance of 25Cr-3.5Mo-6Ni and 25Cr-4.5Mo-6Ni cast duplex stainless steels. *Duplex Stainless Steels,* ASM, pp. 431–444.

16. Liljas, M., and Qvarfort, R. 1986. Influence of nitrogen on weldments in UNS S31803. *Conf. Proc. Duplex Stainless Steel '86,* Hague, Netherlands Institute of Welding, pp. 244–256, Paper 2.

17. Takalo, T. Suutala, N., and Moisio, T. 1979. Austenitic solidification mode in austenitic stainless steel welds. *Met. Trans. A* 10A(8):1173–1181.

18. Suutala, N., Takalo, T., and Moisio, T. 1980. Ferritic-austenitic solidification mode in austenitic stainless steel welds. *Met. Trans. A* 11A(5):717–725.

19. Lippold, J. C., and Savage, W. F. 1980. Solidification of austenitic stainless steel weldments: Part 2—the effect of alloy composition on ferrite morphology. *Welding Journal* 59(2):48-s to 58-s.

20. Brooks, J. A., Williams, J. C., and Thompson, A. W. 1983. STEM analysis of primary austenitic solidified stainless steel welds. *Met. Trans. A* 14A(1):23–31.

21. Brooks, J. A., Williams, J. C., and Thompson, A. W. 1983. Microstructural origin of the skeletal ferrite morphology of austenitic stainless steel welds. *Met. Trans. A* 14A(7):1271–1281.

22. Cieslak, M. J., Ritter, A. M., and Savage, W. F. 1982. Solidification cracking and analytical electron microscopy of austenitic stainless steel weld metals. *Welding Journal* 61(1): 1-s to 8-s.

23. Lippold, J. C., and Savage, W. F. 1982. Solidification of austenitic stainless steel weldments: Part 3—the effect of solidification behavior on hot cracking susceptibility. *Welding Journal* 61(12):388-s to 396-s.

24. Garner, A. 1979. The effect of autogenous welding on chloride pitting corrosion in austenitic stainless steels. *Corrosion* 35(3):108–114.

25. Ogawa, T., Aoki, S., Sakamoto, T., and Zaizen, T. 1982. The weldability of nitrogen-containing austenitic stainless steel: Part 1—chloride pitting corrosion resistance. *Welding Journal* 61(5):139-s to 148-s.

26. Lippold, J. C., Juhas, M. C., and Dalder, E. N. C. 1985. The relationship between microstructure and fracture behavior of fully austenitic Type 316L weldments at 4.2 K. *Met. Trans. A* 16A(10):1835–1848.

27. Ogawa, T., and Koseki, T. 1988. Weldability of newly developed austenitic stainless alloys for cryogenic service: Part II—high-nitrogen stainless steel weld metal. *Welding Journal* 67(1):8-s to 17-s.

28. Suutala, N., Takalo, T., and Moisio, T. 1979. Single-phase ferritic solidification mode in austenitic-ferritic stainless steel welds. *Met. Trans. A* 10A(8):1183–1190.

29. Nelson, D. E., Baeslack III, W. A. and Lippold, J. C. 1985. Characterization of the weld structure in a duplex stainless steel using color metallography. *Metallography* 18:215–225.

30. Taguchi, I., and Hamada, H. 1985. Development of new computer-aided micro-analyzer and its application to iron and steel analysis. *Analytical Sciences* 1: pp. 119–121.

31. Taguchi, I., Hamada, H., and Tani, S. 1985. Development and application of computer-aided micro analyzer (CMA) to analysis of iron and steel. Nippon Steel Technical Report No. 26:59–68.

32. Fredriksson, H. 1979. Transition from peritectic to eutectic reaction in iron-base alloys. *Solidification and Casting of Metals,* The Metals Society pp. 131–138.

33. Lippold, J. C., and Savage, W. F. 1979. Solidification of austenitic stainless steel weldments: Part I—A proposed mechanism. *Welding Journal* 58(12):362-s to 374-s.

34. Murray, W. D., and Landis, F. 1959. Numerical and machine solutions of transient heat-conduction problems involving melting or freezing. *Trans.* ASME 81(5):106–112.

35. *Metal Data Book,* 2nd edition, 1984. Japan Institute of Metals, pp. 25–26.

36. Hertzman, S., Roberts, W., and Lindenmo, M. 1986. Microstructure and properties of nitrogen alloyed duplex stainless steel after welding treatment. *Conf. Proc. Duplex Stainless Steel '86,* Hague, Netherlands Institute of Welding, pp. 257–267, Paper 30.

37. Streicher, M. A. 1956. Pitting corrosion of 18Cr-8Ni stainless steels. *J. Electrochem. Soc.* Vol. 103, pp. 375–390.

38. Dundas, H. J., and Bond, A. P. 1975. Effect of delta ferrite and nitrogen content on the resistance of austenitic stainless steels to pitting corrosion. *Corrosion Forum '75.* Ontario, Canada, NACE. Paper No. 159.

39. Suutala, N., and Kurkela, M. 1985. Localized corrosion resistance of high alloy austenitic stainless steels and welds. *Proc. Conf. Stainless Steels '84,* The Institute of Metals, pp. 240–247.

40. Masumoto, T., and Imai, Y. 1969. Structural diagrams and tensile properties of the 18Cr-Fe-Ni-N quaternary system alloys. *Journal of the Japan Institute of Metals* 33(12):1364–1371 (in Japanese).

Appendix

It was assumed that a prior ferrite grain was a cylindrical shape having the radius of R, and the transformation occurred radially from the grain boundary toward the inside with a concentric, smooth interface.

When the α/γ interface is located at $r = r^*$, the diffusion in the radial direction of nitrogen in ferrite and austenite are given by the following equations, respectively:

in ferrite

$$\frac{\partial C}{\partial t} = D_N^{\alpha}\left(\frac{\partial^2 C}{\partial r^2} + \frac{\partial C}{r\partial r}\right),\ 0 < r < r^* \qquad (1)$$

in austenite

$$\frac{\partial C}{\partial t} = D_N^{\gamma}\left(\frac{\partial^2 C}{\partial r^2} + \frac{\partial C}{r\partial r}\right),\ r^* < r < R \qquad (2)$$

where C is the concentration of nitrogen, and D_N^{α} and D_N^{γ} are the diffusion coefficients of nitrogen in ferrite and austenite, respectively. For the sake of simplicity, the data in pure α iron and γ iron were employed, *i.e.:*

$$D_N^{\alpha} = 1.13\times10^{-6}\ \exp(-41800\ (1 - 14.03/T)/T)\ (m^2/s) \qquad (3)$$

$$D_N^{\gamma} = 3.6\times10^{-5}\ \exp(-79000/T)\ (m^2/s) \qquad (4)$$

where T is the absolute temperature (K).

At the advancing α/γ interface, the conservation of the solute, nitrogen, requires:

$$(C_\gamma^* - C_\alpha^*)\frac{\partial r^*}{\partial t} = D_N^{\gamma}\frac{\partial C}{\partial r}\Big|_{r = r^* + 0} - D_N^{\alpha}\frac{\partial C}{\partial r}\Big|_{r = r^* - 0} \qquad (5)$$

where C_α^* and C_γ^* are the concentrations of nitrogen in ferrite and austenite, respectively, at the interface, and combined by using the partition ratio, K_N, as follows:

$$D_\gamma^* = K_N\, C_\alpha^* \qquad (6)$$

Since few data were reported on the partition ratio of nitrogen (K_N) between the phases, it was roughly determined as 10, with reference to the work by Masumoto (Ref. 40). Other boundary conditions required are:

$$\frac{\partial C}{\partial r}\Big|_{r = 0} = 0 \qquad (7)$$

$$\frac{\partial C}{\partial r}\Big|_{r = R} = 0 \qquad (8)$$

The moving-grid method of Murray and Landis (Ref. 34) used in the present calculation required the existence of both phases, *apriori.* Thereby, the austenite with thickness of 0.1 μm was assumed to be at the grain boundary (*i.e.,* $r^* = 199.9$ μm), and to impart the slight concentration difference of nitrogen (0.001 wt-%) at the α/γ interface. The initial conditions are:

$C = 0.12$ wt-%, $0 < r < r^*,\ r^* < r < R,\ t = 0$ (9)

$C_\alpha^* = 0.119$ wt-%, $r = r^*,\ t = 0$ (10)

$C_\gamma^* = 0.121$ wt-%, $r = r^*,\ t = 0$ (11)